14th IEA Heat Pump Conference
15-18 May 2023, Chicago, Illinois

Modelling and Simulation of a Thermoelectric Heat Pump with Micro-Channel Heat Transfer

Hanlong Wan*, Bo Shen, Kyle R. Gluesenkamp, Zhenning Li

Oak Ridge National Laboratory, Oak Ridge, TN 37831, USA

Abstract

Thermoelectric heat pumps (TEHPs) have advantages of modularity and simple design for heating and cooling in some applications. Models of thermoelectric (TE) heat pumps are widely studied. Nevertheless, most existing modeling work focuses on the TE material or air-sourced TE modules. TEHP modeling, especially the relationship between modules and heat exchangers, has not been comprehensively conducted. This work presents a water-to-water TEHP modeling framework that combines Goldsmid's approach for TE material performance, Gnielinski's correlation for convective heat transfer, and thermal balance theory for heat exchange networks. This combined framework provides an accurate theoretical analysis of the water-to-water TEHP system. Subsequently, the framework was used to empirically determine TE material properties (electric resistivity, thermal conductivity, and Seebeck coefficient) that minimize modeling errors versus experimentally observed values from the literature. Finally, an additional set of experimental TEHP data was used to validate the model, all with relative absolute deviations of approximately 10% when predicting heating capacity and 10%–20% when forecasting cooling capacity at a 30 K temperature lift. For future work, people can further develop models of TEHPs with an air-based heat sink on one side and water channels on the other side.

Selection and/or peer-review under the responsibility of the organizers of the 14th IEA Heat Pump Conference 2023.

Keywords: thermoelectric, heat pump, Seebeck coefficient, coefficient of performance;

1. Introduction

In the 1950s, thermoelectric (TE) techniques were originally studied [1]; later, their applications for heat pumps were taken into consideration [2]. TE modules provide benefits such as cheap cost, modularity, easy design, and environmental friendliness [1] while being less efficient than conventional vapor-compression heat pumps [3]. As a result, there has been an increase in interest in using TE modules for applications like building heating and cooling [4–7], refrigeration [8], personal thermal comfort [9], electronics cooling [10], and clothes dryers [11,12].

Some researchers treated the TE modules' lumped property parameters (Seebeck coefficient S, thermal conductivity K, and electrical resistance *R*) as temperature-dependent. For instance, Nemati et al. estimated the property parameters using a second-order polynomial correlation with the mean temperatures of the hot and cold sides of the TEHP [13]. However, they neglected to take into account the variation in samples and measurements and instead utilized the coefficients from a study that was published in 2020 [14], which were generated using a different TE module. The identical techniques and coefficients were used by Kaushik et al.

* Corresponding author. *E-mail address:* wanh@ornl.gov.

and Feng et al.[15,16]. The attributes were handled as a function of the hot-side temperature by Chen and Snyder et al. [17,18]. Their coefficients, which came directly from the producers, were more trustworthy.

Other researchers treated all or some of the parameters as temperature-independent. Cai et al. treated the properties as constants from the manufacturers' datasheets [19]. Patel et al. treated S and K as constants but the electric resistance *R* as a linear function of the temperature difference between the hot and the cold sides [11].

This paper used Cheon's model [18] to evaluate TE property parameters. In addition, by plugging in the property parameters and applying Goldsmid's method [21] and Gnielinski's correlation [22], this paper developed a detailed liquid-to-liquid TEHP model. Furthermore, the proposed model was validated through quasi-steady-state data from a laboratory test.

2. Methodology

Water-to-water TEHPs, which are simply built and often used in several investigations, is the subject of this study [11,20]; an example is shown in Fig.1. Two mini-channel heat exchangers containing fluid (for example, water) were put on the two sides of one or more TE modules for the TEHP in this investigation. A short distance was maintained between the hot and cold mini-channel heat exchangers using an aluminum space block. UA_{hw} and UA_{cw} are the overall heat transfer coefficients and area of the hot side and cold side, respectively. The model is broadly applicable to scenarios involving liquid-to-liquid, liquid-to-air, and air-to-air interactions thanks to the use of various UA values. This work developed and validated a thermodynamic model using a water-to-water TEHP as a case study. The temperature and UA variables used are marked in Fig.1., as well.

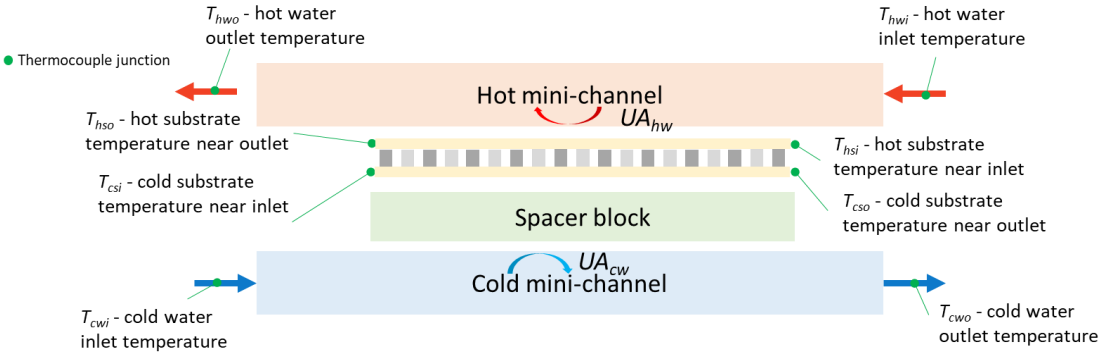

Fig. 1. A general liquid-to-liquid TEHP schematic.

The inlet and outlet water temperatures in the TEHP system under consideration were relatively similar (within 1 K). Thus, the system was made simpler by using lumped approaches. T_h and T_c are the lumped hot- and cold-side temperatures of the TE modules, respectively. The TE surface temperatures can be estimated by measuring the substrate temperatures near the inlet and outlet.

$$T_h \approx \frac{T_{hsi} + T_{hso}}{2} \tag{1}$$

$$T_c \approx \frac{T_{csi} + T_{cso}}{2} \tag{2}$$

Similarly, the lumped hot and cold side water temperatures can be estimated using the inlet and outlet water temperatures.

$$T_{cw} \approx \frac{T_{cwi} + T_{cwo}}{2} \tag{3}$$

$$T_{hw} \approx \frac{T_{hwi} + T_{hwo}}{2} \tag{4}$$

2.1. TE module model

Goldsmid's method is commonly agreed upon and used to describe TE module performance [21]. The heat transfer across the cold side and hot side of one TE module can be given by

$$Q_c = Q_{c\_GS} = SIT_c - \mathrm{K}(T_h - T_c) - I^2 R/2 \quad (5)$$

$$Q_h = Q_{h\_GS} = SIT_h - \mathrm{K}(T_h - T_c) + I^2 R/2 \quad (6)$$

where Q_{c_GS} and Q_{h_GS} are the predicted heat capacities across the cool and hot sides, respectively, and I is the current. When multiple modules are used in one TEHP, the capacity needs to be multiplied by the number of the modules used, or the number of models should be connected and iterated in series.

From Goldsmid's method [21], the lumped parameters (S, R, and K) can be expressed by the parameters of the couples in one module:

$$Af = N \cdot (A_n + A_p) \quad (7)$$

$$S = N \cdot \alpha_i = N \cdot 2\alpha \quad (8)$$

$$R = N \cdot R_i = N \cdot \left(\frac{l_n \rho_n}{A_n} + \frac{l_p \rho_p}{A_p} + R_l\right) = \frac{N^2 l}{Af} 4\rho \quad (9)$$

$$\mathrm{K} = N \cdot \mathrm{K}_i = N \cdot \left(\frac{A_n \kappa_n}{l_n} + \frac{A_p \kappa_p}{l_p}\right) = \frac{Af}{l}\kappa \quad (10)$$

where *N* is the couple number; Af is the packing area of the TE module; ρ, κ, and α are the property parameters of the nodes; and l and A are the geometry parameters of the nodes. We can assume the following:

$$l_p = l_n = l \quad (11)$$

$$A_n = A_p = d_1 d_2 \quad (12)$$

Cheon's model was applied in the proposed model [18]. From the manufacturer's specifications, ΔT_{max}, I_{max}, and $\dot{Q}_{max}$ (performance parameters of TE modules, which are commonly given in the specifications) are 70 K, 8.4 A, and 90 W, respectively, when T_h equals 27°C, and they are 83 K, 8.4 A, and 98 W, respectively, when T_h equals 50°C. The literature indicates that ΔT_{max} was related to T_h by Eq. (13) (Z is the effective device figure of merit) [18]. The linear interpolation method was used to predict $\dot{Q}_{max}$ at other hot-side temperature points.

$$\Delta T_{\max} = \left(T_h + \frac{1}{Z}\right) - \sqrt{\left(T_h + \frac{1}{Z}\right)^2 - {T_h}^2} \quad (13)$$

The node properties can be achieved using the following equations:

$$\alpha = \frac{\dot{Q}_{max}(T_h - \Delta T_{max})}{N T_h^2 I_{max}} \quad (14)$$

$$\rho = \frac{Af(T_h - \Delta T_{max})^2}{2T_h^2 l} \frac{\dot{Q}_{max}}{N^2 I_{max}^2} \quad (15)$$

$$\kappa = \frac{l(T_h - \Delta T_{max})^2}{Af T_h^2} \frac{\dot{Q}_{max}}{\Delta T_{max}} \quad (16)$$

By plugging in the properties, the lumped parameters can be obtained. In the process, the Af is eliminated, and thus, the lumped parameters are not related to Af directly. When the modules' hot side surface temperature varies from 27 °C to 50 °C, the S, R, and K will be in the range of 0.054–0.054 V·K−1, 1.42–1.57 Ω, and 0.633–0.706 W·m−1·K−1, respectively. S changes very small (less than 1%) in the temperature difference range.

2.2. Heat convection model

In this case study, to estimate UA, the heat transfer coefficient between the fluid and the inner surface of the channel was predicted using Gnielinski's correlation [22]. For different fluid regimes and channel geometries, other appropriate correlations [23] can be used to predict the heat transfer coefficient.

$$Nu = \frac{UA \cdot L}{k_w A} = \frac{(f/8)(Re - 1000)\mathrm{Pr}}{1 + 12.7(f/8)^{1/2}(\mathrm{Pr}^{2/3} - 1)} \quad (17)$$

$$f = (0.79\ln(Re) - 1.64)^{-2} \quad (18)$$

$$Pr = \frac{c_p \mu_w}{k_w} \quad (19)$$

$$Re = \frac{\rho_w u L}{\mu_w} \tag{20}$$

μ_w is the dynamic viscosity of water and is a function of water temperature. u is the water flow speed and can be calculated from m_h and m_c. c_p is the specific heat of water, k_w is the thermal conductivity of water, L is the characteristic linear dimension (the inner height of the mini-channel in this study), Re is the Reynolds number, Pr is the Prandtl number; and Nu is the Nusselt number.

2.3. TEHP model

The proposed TEHP model used any two temperatures in $T_{cwi}, T_{cwo}, T_{hwi}, T_{hwo}$ as the inputs and could predict the other two temperatures and the system performance. Fig.2. shows the thermal resistance network of the system and the modeling flow.

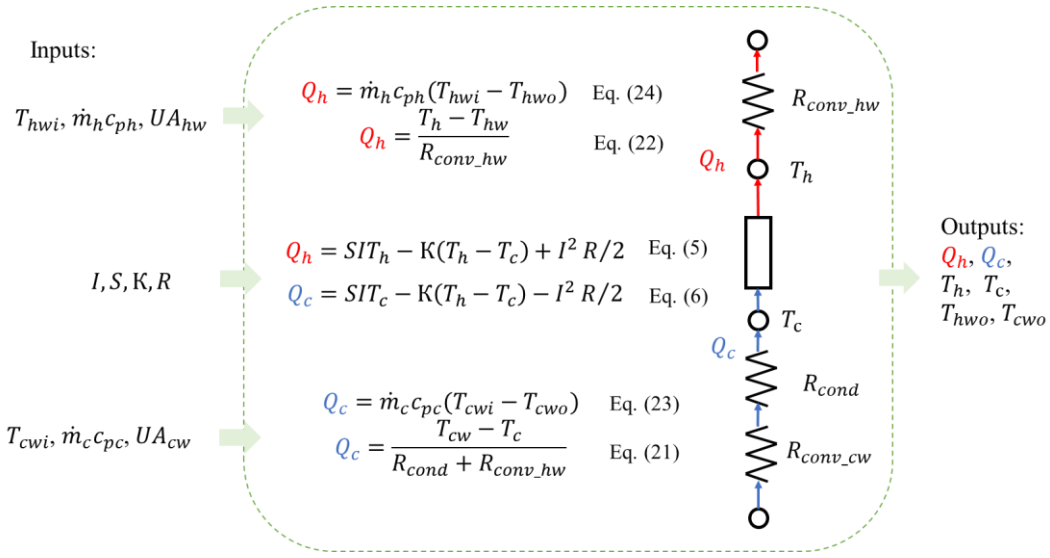

Fig. 2. Resistance network and model flow diagram.

The thermal resistance of the aluminum space block was very small (UA_{hot} is about 8 W/K, while UA_{block} equals 188 W/K) and could be ignored in the analysis. The cooling capacity and heating capacity can be derived as follows:

$$Q_c = \frac{LMTD_c}{\frac{l_s}{k_{alu}A_s} + \frac{1}{UA_{cw}}} \approx UA_{cw}(T_{cw} - T_c) = \frac{T_{cw} - T_c}{R_{cond} + R_{conv\_hw}} \tag{21}$$

$$Q_h \approx UA_{hw}(T_h - T_{hw}) = \frac{T_h - T_{hw}}{R_{conv\_hw}} \tag{22}$$

LMTD is the log mean temperature difference. Considering the water temperature change,

$$Q_c = \dot{m}_c(h_{cwo} - h_{cwi}) \cong \dot{m}_c c_p(T_{cwo} - T_{cwi}) \tag{23}$$

$$Q_h \cong \dot{m}_h c_p(T_{hwi} - T_{hwo}) \tag{24}$$

$\dot{m}$ is the mass flow rate of the water, and h is the enthalpy of the water, and c_p is the specific heat of water. Since the channel surface temperature and the fluid temperature are close and no phase change exists, the capacity can be simplified using Eqs. (11) and (12). Water was used in this study, and its specific heat was treated as a constant. Using Eqs. (1)–(6) and Eqs. (11)–(14) and knowing property parameters and UA values, all the temperature variables can be solved.

2.4. Data source

A dishwasher using TEHPs was developed by the authors' group [24]. Two TEHPs were used in the dishwasher, and transient laboratory test data from one of the TEHPs were used to validate the proposed model. Compared with the quasi-steady-state TEHP testing previously described, in this testing, two space blocks

were used for each TE module. However, the conductivity of the space blocks is very high, so the resistance can be ignored, and the same model can be applied. In addition, the TEHPs used in this project contained five TE modules.

3. Results and discussion

The results of the transient testing are plotted in Fig.3.

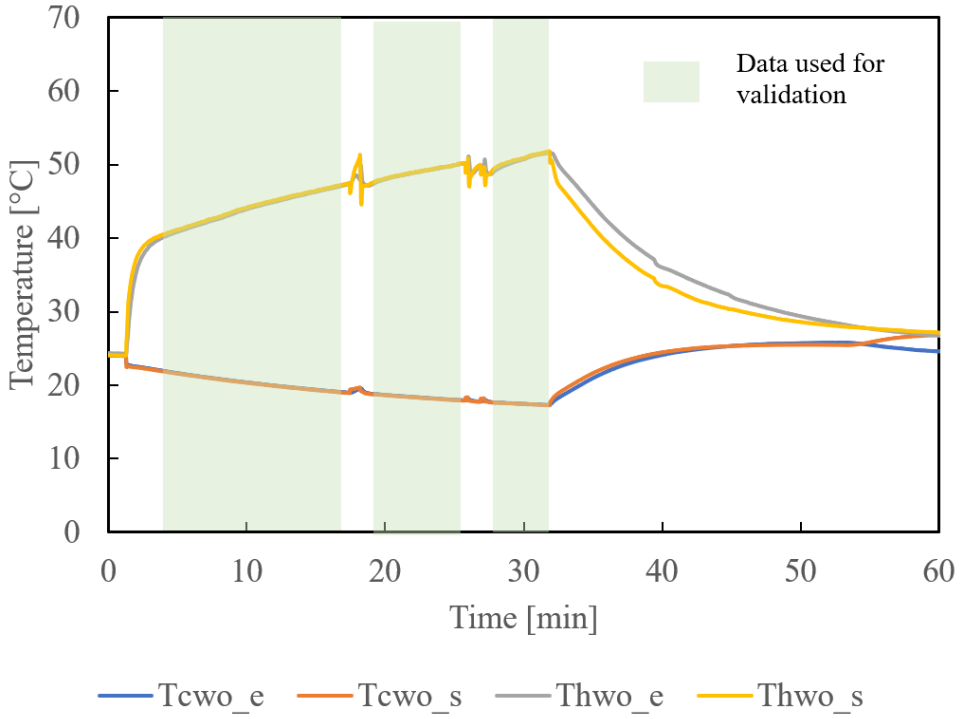

Fig. 3. Experimental and model-predicted outlet water temperature.

When the TE module is on (i.e., the current passing through the module is greater than 0) and the system is stable, the model has good agreement with the measured values. However, when the module is off, the model cannot predict the outlet conditions perfectly because the thermal mass of the system is not considered in the model. Thus, when the module is off, the predicted temperature of the TE module changes immediately and causes water temperature to change at the same time. However, because of the system's thermal mass, the experimental water temperature change is delayed.

Unlike in the steady-state test, some noise exists in the temperature signals. The data with positive current were screened out, and the outliers were excluded (as shown in the shaded area in Fig.3.). The performance of the models using the data set is listed in Table 1. The results are close for all three approaches, which implies that the slight change in the parameters (S, R, and K) will not significantly affect the model. The hot- and cold-side temperatures of the TE module were not predicted perfectly because the temperature sensors installed may not reflect the lumped surface temperature of the modules.

Table 1. TEHP model performance

RME_{DT} (%)	RME_{DT_w} (%)	RME_{Q_c} (%)	RME_{Q_h} (%)	COP_c(-)
35.10	0.61	7.09	8.84	0.6

Table 2 provides the systematic uncertainty of measured and derived values. Using the information from the quasi-steady-state TEHP test and Lecompte's approach [24], Propagated uncertainties of the resulting values were computed. The uncertainty of capacity computed from the water side is high due to the low accuracy of thermocouples and the tiny difference between the input and output water temperatures.

Comparatively, the projected cooling capacity was just 50 W. Therefore, utilizing the water-side capacity to calculate the system coefficient of performance (COP) and assess the performance of the models would not yield useful information. On the other hand, the calculation of capacity from the TE module side has little uncertainty when all of the TE material parameters are accurate. The TE hot- and cold-side temperature measurements have the biggest impact on the TE module performance uncertainty. As a result, a suitable metric for assessing the performance of the models is the difference between the measured and simulated TE module surface temperature. A more accurate system COP may also be obtained by computing COP using the TE module-side capacity. Experiments will be conducted in future with RTDs for better water side capacity accuracy.

Table 2. Uncertainties of measured and derived quantities

	Quantity	Instrument	Uncertainty
Measurement	Geometry	Vernier Caliper	±0.02 mm
	Temperature	Omega TMQSS-062G-6 Type T thermocouple read by NI 9214 module	±0.5 K
	Mass flow rate (water)	Bronkhorst M-15 Coriolis flowmeter	±0.5%
	Applied voltage to TE banks	Sorensen XG150-5.6 DC Programmable Power Supply	±2 V
	Current through TE banks	Sorensen XG150-5.6 DC Programmable Power Supply	±0.05 A
Derived quantity	Capacity (water side)	N/A	±40 W
	Capacity (TE module side)	N/A	±0.5 W
	TE power	N/A	±10 W

4. Conclusions

A thorough modeling framework was given in this study based on a numerical method that incorporates three sub-models: Goldsmid's method for TE material performance, Gnielinski's correlation for convective heat transfer, and thermal balance theory for a heat exchange network. Using this modeling framework, a water-to-water TEHP system was precisely assessed. The TE material performance was estimated through Cheon's model. Finally, quasi-steady-state experimental data were used to validate the overall modeling framework. The findings are as follows:

- The proposed water-to-water TEHP model can achieve a *RME* of approximately 10% when predicting heating capacity and 10%–20% when forecasting cooling capacity at a 30 K temperature lift. For larger lifts, the cooling capacity becomes small, and the relative uncertainty in cooling capacity gets larger.
- TE surface temperatures have a major impact on the TEHP capacity and efficiency. In contrast, the impact of temperature-based variations in TE material properties was minor, over the evaluated range of 20 to 50 °C.
- It is common in TEHP applications to have small changes in water temperature across the TE, leading to difficulty in accurately measuring water-side capacity. This work allows engineers to predict capacities and system COP from knowledge of TE properties and heat transfer, without high accuracy measurements of differential temperatures.

For future work, a more accurate liquid temperature measurement method is needed. Furthermore, customer-designed TE modules are also necessary. Models of TEHPs with an air-based heat sink on one side and water channels on the other side should also be developed.

Nomenclature

A	area (m^2)
c_p	specific heat ($J \cdot kg^{-1} \cdot K^{-1}$)

D	width (m)
d	length of side (m)
DT	temperature difference (K)
f	correction factor
h	enthalpy ($J \cdot kg^{-1}$)
H	height (m)
I	current (A)
k	liquid thermal conductivity ($W \cdot m^{-1} \cdot K^{-1}$)
L	length (m)
l	thickness (m)
m	mass flow rate ($kg \cdot s^{-1}$)
N	number
Nu	Nusselt number
Pr	Prandtl number
Q	capacity (J)
R	lumped electric resistance (Ω)
Re	Reynolds number
RME	relative mean error
S	lumped Seebeck coefficient ($V \cdot K^{-1}$)
T	surface or liquid temperature (K or °C)
TE	thermoelectric
TEHP	thermoelectric heat pump
u	liquid flow speed ($m \cdot s^{-1}$)
UA	heat transfer coefficient and area ($W \cdot K^{-1}$)
Z	effective device figure of merit (K^{-1})

Greek symbols

α	Seebeck coefficient ($V \cdot K^{-1}$)
κ	thermal conductivity ($W \cdot m^{-1} \cdot K^{-1}$)
μ	dynamic viscosity ($kg \cdot m^{-1} \cdot s^{-1}$)
ρ	electric resistivity ($\Omega \cdot m^{-1}$), density ($kg \cdot m^{-3}$)
σ	electrical conductivity ($m \cdot \Omega^{-1}$)
Κ	lumped conductivity ($W \cdot m^{-1} \cdot K^{-1}$)

Subscripts

c	cold side, cooling
exp	experimental
GS	Goldsmid's method
h	hot side, heating
i	inlet
max	maximum
n	n-type node
o	outlet
p	p-type node
s	side
sim	simulation
test	empirical method
w	water

Acknowledgements

This work was sponsored by the US Department of Energy's (DOE's) Building Technologies Office under Contract No. DE-AC05-00OR22725 with UT-Battelle LLC. This research used resources at the Building Technologies Research and Integration Center, a DOE Office of Science User Facility operated by the Oak Ridge National Laboratory. The authors would also like to acknowledge Tony Bouza, Technology Manager – HVAC&R, Water Heating, and Appliance, DOE Building Technologies Office.

References

[1] Riffat SB, Ma X, Wilson R. Performance simulation and experimental testing of a novel thermoelectric heat pump system. Applied Thermal Engineering 2006;26:494–501. https://doi.org/10.1016/j.applthermaleng.2005.07.016.
[2] Rowe DM. Thermoelectrics Handbook: Macro to Nano. Boca Raton, FL: CRC press - Taylor & Francis Group; 2005.
[3] Zhao D, Tan G. A review of thermoelectric cooling: Materials, modeling and applications. Applied Thermal Engineering 2014;66:15–24. https://doi.org/10.1016/j.applthermaleng.2014.01.074.
[4] He W, Zhou J, Chen C, Ji J. Experimental study and performance analysis of a thermoelectric cooling and heating system driven by a photovoltaic/thermal system in summer and winter operation modes. Energy Conversion and Management 2014;84:41–9. https://doi.org/10.1016/j.enconman.2014.04.019.
[5] Ibañez-Puy M, Bermejo-Busto J, Martín-Gómez C, Vidaurre-Arbizu M, Sacristán-Fernández JA. Thermoelectric cooling heating unit performance under real conditions. Applied Energy 2017;200:303–14. https://doi.org/10.1016/j.apenergy.2017.05.020.
[6] Irshad K, Habib K, Basrawi F, Saha BB. Study of a thermoelectric air duct system assisted by photovoltaic wall for space cooling in tropical climate. Energy 2017;119:504–22. https://doi.org/10.1016/j.energy.2016.10.110.
[7] Zhao D, Yin X, Xu J, Tan G, Yang R. Radiative sky cooling-assisted thermoelectric cooling system for building applications. Energy 2019:116322. https://doi.org/10.1016/j.energy.2019.116322.
[8] Liu X, Fu RS, Wang ZQ, Lin L, Sun ZX, Li XL. Thermodynamic analysis of transcritical CO2 refrigeration cycle integrated with thermoelectric subcooler and ejector. Energy Conversion and Management 2019;188:354–65. https://doi.org/10.1016/j.enconman.2019.02.088.
[9] Duan L, Han J, Cao L, Huo C. Experimental study on heat transfer characteristics of CNTs/Al2O3nanofluids in personal cooling system based on thermoelectric refrigeration. Procedia Engineering 2017;205:588–95. https://doi.org/10.1016/j.proeng.2017.10.421.
[10] Liang K, Li Z, Chen M, Jiang H. Comparisons between heat pipe, thermoelectric system, and vapour compression refrigeration system for electronics cooling. Applied Thermal Engineering 2019;146:260–7. https://doi.org/10.1016/j.applthermaleng.2018.09.120.
[11] Patel VK, Gluesenkamp KR, Goodman D, Gehl A. Experimental evaluation and thermodynamic system modeling of thermoelectric heat pump clothes dryer. Applied Energy 2018;217:221–32. https://doi.org/10.1016/j.apenergy.2018.02.055.
[12] Patel V, Gluesenkamp KR. Thermoelectric Heat Pump Clothes Dryer using Secondary Loop Heat Exchangers: Experimental Evaluation and System Modeling, 2018.
[13] Nemati A, Nami H, Yari M, Ranjbar F, Rashid Kolvir H. Development of an exergoeconomic model for analysis and multi-objective optimization of a thermoelectric heat pump. Energy Conversion and Management 2016;130:1–13. https://doi.org/10.1016/j.enconman.2016.10.045.
[14] Xuan XC, Ng KC, Yap C, Chua HT. The maximum temperature difference and polar characteristic of two-stage thermoelectric coolers. Cryogenics 2002;42:273–8. https://doi.org/10.1016/S0011-2275(02)00035-8.
[15] Kaushik SC, Manikandan S, Hans R. Energy and exergy analysis of thermoelectric heat pump system. International Journal of Heat and Mass Transfer 2015;86:843–52. https://doi.org/10.1016/j.ijheatmasstransfer.2015.03.069.
[16] Feng Y, Chen L, Meng F, Sun F. Influences of the Thomson Effect on the Performance of a Thermoelectric Generator-Driven Thermoelectric Heat Pump Combined Device. Entropy 2018;20:29. https://doi.org/10.3390/e20010029.
[17] Chen M, Snyder GJ. Analytical and numerical parameter extraction for compact modeling of thermoelectric coolers. International Journal of Heat and Mass Transfer 2013;60:689–99. https://doi.org/10.1016/j.ijheatmasstransfer.2013.01.020.
[18] Cheon S-Y, Lim H, Jeong J-W. Applicability of thermoelectric heat pump in a dedicated outdoor air

system. Energy 2019;173:244–62. https://doi.org/10.1016/j.energy.2019.02.012.
[19] Cai Y, Zhang D-D, Liu D, Zhao F-Y, Wang H-Q. Air source thermoelectric heat pump for simultaneous cold air delivery and hot water supply: Full modeling and performance evaluation. Renewable Energy 2019;130:968–81. https://doi.org/10.1016/j.renene.2018.07.007.
[20] Kumar N, Gluesenkamp KR, Turnaoglu T, Patel V, Gehl AC, Abuheiba A, et al. Novel Dishwasher with Thermal Storage and Thermoelectric Heat Recovery. Oak Ridge National Laboratory, Oak Ridge, TN (United States); 2021.
[21] Goldsmid H. Thermoelectric Refrigeration. Springer; 2013.
[22] Gnielinski V. Heat Transfer Coefficients for Turbulent Flow in Concentric Annular Ducts. Heat Transfer Engineering 2009;30:431–6. https://doi.org/10.1080/01457630802528661.
[23] Bergman TL, Lavine AS, Incropera FP, DeWitt DP. Introduction to heat transfer. John Wiley & Sons; 2011.
[24] Lecompte S, Gusev S, Vanslambrouck B, De Paepe M. Experimental results of a small-scale organic Rankine cycle: Steady state identification and application to off-design model validation. Applied Energy 2018;226:82–106. https://doi.org/10.1016/j.apenergy.2018.05.103.